

Validation of the CLARA-A3 Top-of-Atmosphere Radiative Fluxes Climate Data Record

TOM AKKERMANS^a AND NICOLAS CLERBAUX^a

^a *Royal Meteorological Institute Belgium, Brussels, Belgium*

(Manuscript received 11 May 2023, in final form 19 September 2023, accepted 12 October 2023)

ABSTRACT: The third edition of the CM SAF Cloud, Albedo and Surface Radiation dataset from AVHRR data (CLARA-A3) contains for the first time the top-of-atmosphere products reflected solar flux (RSF) and outgoing longwave radiation (OLR), which are presented and validated using CERES, HIRS, and ERA5 reference data. The products feature an unprecedented resolution (0.25°) and time span (4 decades) and offer synergy and compatibility with other CLARA-A3 products. The RSF is relatively stable; its bias with respect to (w.r.t.) ERA5 remains mostly within $\pm 2 \text{ W m}^{-2}$. Deviations are predominantly caused by absence of either morning or afternoon satellite, mostly during the first decade. The radiative impact of the Pinatubo volcanic eruption is estimated at 3 W m^{-2} . The OLR is stable w.r.t. ERA5 and HIRS, except during 1979–80. OLR regional uncertainty w.r.t. HIRS is quantified by the mean absolute bias (MAB) and correlates with observation density and time (satellite orbital configuration), which is optimal during 2002–16, with monthly and daily MAB of approximately 1.5 and 3.5 W m^{-2} , respectively. Daily OLR uncertainty is higher (MAB +40%) during periods with only morning or only afternoon observations (1979–87). During the CERES era (2000–20), the OLR uncertainties w.r.t. CERES-EBAF, CERES-SYN, and HIRS are very similar. The RSF uncertainty achieves optimal results during 2002–16 with a monthly MAB w.r.t. CERES-EBAF of $\sim 2 \text{ W m}^{-2}$ and a daily MAB w.r.t. CERES-SYN of $\sim 5 \text{ W m}^{-2}$, and it is more sensitive to orbital configuration than is OLR. Overall, validation results are satisfactory for this first release of TOA flux products in the CLARA-A3 portfolio.

KEYWORDS: Energy budget/balance; Radiative fluxes; Remote sensing; Climate records; Bias; Time series

1. Introduction

Broadband top-of-atmosphere (TOA) outgoing longwave radiation (OLR) and reflected solar flux (RSF) are essential climate variables. High-quality data records of satellite-derived OLR and RSF measurements with sufficient length [Climate Data Record (CDR)] are needed by, among others, the climate modeling and climate monitoring communities, preferably spanning several decades.

To this end, there are three main approaches: A first approach consists in dedicated ERB missions with broadband (BB) radiometers providing integrated observations of the radiation over large parts of the electromagnetic spectrum: “shortwave” ($0.3\text{--}4 \mu\text{m}$) and “longwave” ($4\text{--}50 \mu\text{m}$). A second approach consists in radiative transfer calculations based on cloud observations and atmospheric reanalysis. As a third approach, a so-called narrowband-to-broadband conversion can be used to directly estimate broadband TOA radiation from narrowband weather satellite observations taken at different wavelengths in the spectrum (visible and infrared).

Using this third approach, new RSF and OLR data records are generated as part of the third edition of the CM SAF Cloud, Albedo and Surface Radiation dataset from AVHRR data (CLARA-A3; Karlsson et al. 2023a,b), featuring a fine


spatial resolution ($0.25^\circ \times 0.25^\circ$) and long time span (42 yr). The first and second CLARA editions were described by Karlsson et al. (2013, 2017), respectively, and did not yet include TOA radiative fluxes. The newly generated RSF and OLR data record’s retrievals and processing chains are documented by Akkermans and Clerbaux (2021) for the RSF and Clerbaux et al. (2020) for the OLR, each also including a preliminary validation on a limited amount of generated data.

This paper presents and validates the CLARA-A3 RSF and OLR data records on their full time span (1979–2020). This is done primarily by comparing with reference data records of proven quality and accuracy, but with shorter time span and/or coarser spatial resolution. Section 2 provides an overview of the different reference data records used for intercomparison. Section 3 describes the validation method, including the terminology, the applied statistical metrics, the data visualization, and the temporally varying orbital configuration of the satellite constellation used to derive the CLARA-A3 data record. The validation results are presented and discussed in section 4 (RSF) and section 5 (OLR), each describing the stability as well as the regional uncertainty of the data record. This is followed by section 6, which provides a spatial view on the validation. Section 7 summarizes and concludes the paper and offers an outlook for further research.

2. Reference data records used in the validation

a. CERES SYN1deg Ed.4.1 (daily and monthly)

The Clouds and the Earth’s Radiant Energy System (CERES; Wielicki et al. 1996) product SYN1deg Ed4.1 provides estimates of the daily and monthly mean RSF and OLR fluxes from

 Denotes content that is immediately available upon publication as open access.

Corresponding author: Tom Akkermans, tom.akkermans@meteo.be

March 2000 onward at a $1^\circ \times 1^\circ$ latitude–longitude resolution. The products consist of CERES-observed (i.e., real broadband measurement), geostationary enhanced and temporally interpolated TOA radiative fluxes. Given the sun-synchronous orbits of the CERES instruments on board the *Aqua* and *Terra* satellites, the observations are performed only twice per day. Therefore, hourly TOA fluxes and cloud properties from five contiguous geostationary imagers, covering 60°S – 60°N at any given time, are used for an improved modeling of the diurnal variability between the CERES observations (Doelling et al. 2013). While the SYN1deg approach provides improved diurnal coverage by merging CERES and 1-hourly geostationary (GEO) data, artifacts in the GEO imager visible bands over certain regions and time periods can introduce larger regional uncertainties. Spurious jumps in the SW TOA flux record can occur when GEO satellites are replaced, because of changes in satellite position, calibration, visible sensor spectral response, cloud retrieval quality, and imaging schedules. Such artifacts in the GEO data can be problematic in studies of TOA radiation interannual variability and/or trends (Loeb et al. 2018). The issue does not play a role in the longwave product, given the general stability of GEO infrared bands due to onboard blackbody sources for calibration. In practice, CERES SYN1deg is still the best reference data record to validate daily TOA fluxes. It is used for the validation of daily and monthly global mean fluxes, from which the temporal variability determines the stability of the data record. It is used as well for the validation of processing error, containing the remaining random and systematic errors, which is performed at gridbox level and therefore considered a validation of spatial patterns (also referred to as regional uncertainty). For this, the SYN1deg product is suitable given its high spatiotemporal resolution (combination of GEO data). The largest disadvantage is the record's time span, which is limited to 2000–20, a period that is therefore referred to as the “CERES era,” in contrast to the period 1979–99 (“pre-CERES era”). The data are downloaded from the “CERES Ordering Tool” web portal (<https://ceres-tool.larc.nasa.gov/ord-tool/>). CERES products based on *Terra* and/or *Aqua* satellites suffer from data gaps in certain periods. As a consequence, three *Terra*-only months are not used for validation purposes (August 2000, June 2001, March 2002). The impact of gaps after July 2002 is lower because since then the CERES products have been composed of both *Terra* and *Aqua* satellite orbits.

b. CERES EBAF Ed.4.1 (monthly)

The CERES Energy Balanced and Filled (EBAF) Ed.4.1 data record (Loeb et al. 2018) provides state-of-the-art estimates of monthly mean RSF and OLR fluxes from March 2000 onward at a $1^\circ \times 1^\circ$ latitude–longitude resolution. The longwave monthly mean EBAF product is computed directly from SYN1deg daily mean product, given the abovementioned stability of the GEO imager infrared bands. For the shortwave (SW) TOA fluxes, to maintain the diurnal information found in SYN1deg, but also preserve the excellent CERES instrument calibration stability (at their sun-synchronous observation times), the EBAF product introduced a new approach involving diurnal correction ratios (DCRs) to convert daily regional mean SSF1deg SW fluxes into

diurnally complete values, analogous to SYN1deg but without geostationary artifacts (Loeb et al. 2018). Furthermore, even with the most recent CERES Ed4 instrument calibration improvements, the SYN1deg Ed4 net imbalance is still about 4.3 W m^{-2} , much larger than the expected observed ocean heating rate of about 0.71 W m^{-2} (Johnson et al. 2016). Therefore, the CERES EBAF dataset uses an objective constraint algorithm (Loeb et al. 2009) to adjust SW and LW TOA fluxes within their ranges of uncertainty to remove the inconsistency between average global net TOA flux and heat storage in the Earth-climate system, mostly in the oceans. CERES EBAF is used for monthly global mean validation (stability) as well as for processing error validation (regional uncertainty). The record's time span is identical to the SYN1deg product, as is the record's download location (<https://ceres-tool.larc.nasa.gov/ord-tool/>).

c. HIRS OLR daily v01r02

The NOAA National Centers for Environmental Information (NCEI) provides a high quality CDR of OLR (Lee et al. 2007, 2014). Level-1b all-sky data from the High Resolution Infrared Radiation Sounder (HIRS) instrument are the main input into the daily OLR record. The data record is produced by applying a combination of statistical techniques, including narrowband-to-broadband regression, instrument ambient temperature prediction coefficients, and intersatellite bias corrections. The HIRS OLR daily data record is characterized by a global coverage, a $1^\circ \times 1^\circ$ equal-angle grid resolution, and a temporal coverage from 1979 until present. The OLR estimated from imagers' radiance observations on board operational geostationary satellites (via the GridSat CDR; Knapp et al. 2011) and the GOES Surface and Insolation Product (GSIP; Kondratovich 2013) is incorporated to allow an accurate temporal integration of the daily mean OLR. Since polar areas (about 60° poleward) are not covered by geostationary observations, only HIRS observations are used to derive the daily OLR in these regions. The HIRS OLR estimation technique has been vigorously validated against the Earth Radiation Budget Experiment (ERBE) and CERES data (Ellingson et al. 1994; Lee et al. 2007). The HIRS OLR daily data record is in this paper used for daily and monthly global mean validation (stability), as well as for processing error validation (regional uncertainty) given its high spatiotemporal resolution (combination with GEO data). In contrast to the state-of-the-art CERES products, it is available for the entire time span of the CLARA-A3 record (1979–2020), making it the main reference data record for the OLR stability. In practice, it is used to verify whether the CERES performance is maintained backward in time, that is, during the pre-CERES era. The monthly mean OLR is calculated by temporally aggregating the daily mean OLR. The data are downloaded from the “UMD OLR CDR Portal” (<https://olr.umd.edu/>). In figures and tables, this reference data record is also referred to as “HIRS.” A potential weakness of validating with HIRS is that the HIRS instruments are on the same drifting (in local time) satellite orbits as the AVHRR instrument.

d. HIRS OLR monthly v02r07

The HIRS OLR monthly data record shares the same basic characteristics as the HIRS OLR daily record, described in

section 2c. The data record uses the level-1b HIRS data as main input and is produced by applying the same combination of statistical techniques. However, the HIRS OLR monthly time series is generated on a $2.5^\circ \times 2.5^\circ$ equal-angle grid. In addition, the monthly OLR CDR is estimated from the HIRS all-sky radiance observations directly and does not use geostationary observations, which results in a more consistent time series, as there are no data gaps due to unavailability of geostationary satellites (e.g., during most of the year 1985). These data are used to address the stability of the monthly mean CLARA-A3 OLR products, but they are not used for regional validation because of their low resolution. The data have been downloaded from the “UMD OLR CDR Portal” (<https://olr.umd.edu/>). In figures and tables, this reference data record is referred to as “HIRS-MM.”

e. ERA5

ERA5 is the fifth atmospheric reanalysis from ECMWF (Hersbach et al. 2020). The data record provides a physically consistent blend of forecast and observations, resulting in a spatially and temporally seamless coverage. The model consists of the Integrated Forecasting System (IFS) cycle 41r2 with a four-dimensional variational analysis (4DVAR) assimilation system. The output has a temporal resolution of 1 h, and a reduced Gaussian spatial grid, which is bilinearly interpolated on a regular latitude/longitude grid of $0.25^\circ \times 0.25^\circ$. The radiation scheme of ERA5 is described in Hogan and Bozzo (2018). The record’s total time span is 1959–2020. Given the physical consistency throughout the record, ERA5 is selected for long-term global mean bias validation: it is useful to assess the stability of CLARA-A3’s data record, especially when there is no other reference data record available, as is the case for RSF. On the other hand, ERA5 is a reanalysis product with a significant modeling component: It drastically underperforms in short-term spatially explicit comparisons (large instantaneous biases on gridbox level, which cancel out on longer temporal and spatial scales), making it not useful for processing error validation at regional scale. The data have been collected from the Copernicus Climate Data Store (available online: <https://cds.climate.copernicus.eu>).

f. ISCCP-FH and Cloud-CCI

The International Satellite Cloud Climatology Project FH product (ISCCP-FH) (Young et al. 2018; Zhang et al. 2019) is in essence a cloud product with TOA fluxes calculated from the retrieved cloud properties using a radiative transfer model (RadH-PRD). For the cloud retrievals, ISCCP-FH uses a composite of polar and geostationary satellites. The ISCCP-FH data are provided on a $1^\circ \times 1^\circ$ latitude–longitude grid, and have been downloaded from https://isccp.giss.nasa.gov/pub/flux-fh/tar-nc4_MPF/.

Similar to ISCCP-FH, the Cloud-CCI data record (Stengel et al. 2020) is in essence a cloud product with TOA fluxes calculated from the retrieved cloud properties using the BUGSrad radiative transfer model. For the cloud retrievals, Cloud-CCI (L3C AVHRR-PM v3.0) is based purely on AVHRR afternoon satellites. The Cloud-CCI data are provided on a $0.5^\circ \times 0.5^\circ$

latitude–longitude grid and have been downloaded from https://public.satproj.klima.dwd.de/data/ESA_Cloud_CCI/CLD_PRODUCTS/v3.0/L3C/.

These products are only used to compare the global mean TOA flux (stability) with CLARA-A3 and other data records, and to make a brief assessment of their differences. They are not used for actual validation given their lower performance with respect to the state-of-the-art reference records CERES and HIRS.

3. Method

The three main uncertainty metrics discussed here are the mean bias, the stability, and the processing error (regional uncertainty) of the CLARA-A3 fluxes with respect to the reference data records.

a. Terminology

1) MEAN BIAS

The CLARA-A3 RSF and OLR products rely on empirical relations with CERES products, and hence their absolute radiometric level can be considered “tuned” (not independent). Consequently, no attempt is made to quantify the metric in this paper. Rather than denoting the absolute radiometric error, the term “mean bias” is here used to describe the daily mean overall bias with respect to a reference data record. It is calculated by subtracting the gridded CLARA-A3 flux from a gridded reference data record, which produces a gridded bias (a “bias map”) from which the global spatial average is taken. Depending on the reference data record, this mean bias may have several causes, such as differences in calibration, satellite instruments, time of observation, temporal sampling, which all have in common that they are not random but relatively constant in time and space (although they may slowly evolve in time, e.g., drifting of satellite orbit). Because of its tuned character and given the significant regional bias variations (leading to large compensation effects), the mean bias itself is considered to be a less meaningful “accuracy” metric for the CLARA-A3 TOA flux products. However, it is still interesting to compare the CLARA-A3 mean bias with other data records, that is, how CLARA-A3 and these other data records are scaled in comparison with the absolute level of the CERES products.

2) STABILITY

The stability of the CLARA-A3 data record is evaluated as the maximum variation (maximum–minimum) of the global mean bias over a long period (decades). A stable data record consists of a temporally systematic mean bias. Note that this stability is only relative to the inherent stability of the reference data record. Using different reference records allows attributing observed stability problems to one of these records. Variations or discontinuities, caused by several mechanisms mentioned above for the mean bias [section 3a(1)], should remain within acceptable limits to render the data record useful for climate monitoring purposes.

3) PROCESSING ERROR (REGIONAL UNCERTAINTY)

The second source of uncertainty comes from the processing of AVHRR observations into TOA fluxes. This includes the conversion of the narrowband (channel) observations (reflectances and brightness temperatures) into broadband quantities, the subsequent integration from these directional to hemispherical quantities using angular dependency models (ADMs), and finally the daily and monthly temporal interpolation of these quantities [see Akkermans and Clerbaux (2021) and Clerbaux et al. (2020) for details]. It is the methodology uncertainty, which causes regional flux errors. To quantify this error, the CLARA-A3 products are compared with similar products derived from the CERES instruments at a $1^\circ \times 1^\circ$ spatial scale. CERES is considered as the best reference data to address this accuracy. For OLR, also HIRS is used to assess the processing error during the pre-CERES era (1979–99). In practice, all data records are first regridded on the same nested $1^\circ \times 1^\circ$ latitude–longitude grid as used for the CERES products (see section 3b). Then, the bias-corrected mean absolute value of the difference with the CERES products is evaluated. It is interesting to look at time series of the processing error, to check the consistency over the data record extent, in particular to check that the errors obtained with different satellites (different AVHRR instruments) are consistent with each other. Even after correction for the global mean bias [section 3a(1)], the processing error still contains a considerable regional systematic component: indeed, each grid box has a surface type that is generally invariant in time (e.g., ocean or desert), and in some regions also the cloud cover has a preferential state (e.g., clear sky is dominant in the Sahara Desert). Therefore, scene type dependent errors can be considered regionally systematic errors. This explains the “accuracy” part of the processing error. On the other hand, there is also a random component of the processing error: for instance, errors dependent on viewing and illumination geometry (angular dependent errors). For instantaneous fluxes, or for fluxes integrated on short time scales (e.g., daily mean), these errors can be significant. On longer time scales, for a given location (grid box), these errors cancel each other out since the angles of all observations are not constant but change randomly over time. Indeed, we see that a part of the processing error decreases when calculated on a longer time scale. This explains the “precision” part of the processing error, that is, the random error. Accuracy and precision are therefore assessed together in the combined processing error, and globally integrated with the bias-corrected metric mean absolute bias [MAB; section 3c(2)], which is calculated spatially, that is, over all the grid boxes, and for each time step (daily mean flux, monthly mean flux, etc.). The processing error metric MAB is furthermore an expression of the regional uncertainty in the spatially explicit grid of CLARA-A3 fluxes: it describes to which extent the bias deviates from its mean in the spatial dimension, that is, how spatially homogeneous or heterogeneous the bias is (for a given temporal unit, i.e., for a given map depicting daily or monthly mean flux). The CLARA-A3 flux is provided with an uncertainty range of \pm MAB with 57.5% accuracy, assuming a Gaussian distribution.

b. Maps and grids

Unlike validation of global means, a spatially explicit validation (such as MAB) requires each data record to be aggregated on a common base grid, typically the coarsest one. In this paper the coarse-resolution ($2.5^\circ \times 2.5^\circ$) HIRS-MM OLR monthly v02r07 is not used for the spatially explicit processing error analysis. All other data records were already available in (or were aggregated to) the so-called CERES nested 1.0° grid (<https://ceres.larc.nasa.gov/data/general-product-info/#ceres-nested-10-processing-grid>), which was selected as common base grid.

Since this is an equal-angle grid, global statistical metrics (section 3c) would not represent the true spatial distribution as pixel area decreases poleward. Therefore, a meridionally varying weighting factor w_j , which accounts for the spatial distortion, is applied to the statistical measures, thereby in practice converting the grid to an equal-area grid. The weighting factor is normalized so that its global average equals one.

c. Statistical measures

The retrieved daily mean CLARA-A3 flux F_{CLARA} is validated against the daily mean flux from a gridded reference data record, denoted by F_{REF} . The following statistical measures are used in the validation:

1) BIAS DEFINED PER GRID BOX ($B_{i,j}$)

Prior to the validation, the spatial resolutions of both F_{CLARA} and F_{REF} are first downgraded to match the CERES nested processing grid (section 3b). Maps of their difference are then created (daily “bias maps”), from which a single grid box with latitude and longitude indices (i, j) is calculated as

$$B_{i,j} = F_{\text{CLARA},i,j} - F_{\text{REF},i,j}. \quad (1)$$

The gridbox specific bias is used to calculate the other statistical measures.

2) MB, DEFINED GLOBALLY

The global mean bias (MB) is calculated over all grid boxes’ biases as follows:

$$\begin{aligned} \text{MB} &= \frac{1}{mn} \sum_{i=1}^m \sum_{j=1}^n w_j B_{i,j} \\ &= \frac{1}{mn} \sum_{i=1}^m \sum_{j=1}^n w_j (F_{\text{CLARA},i,j} - F_{\text{REF},i,j}), \end{aligned} \quad (2)$$

where $B_{i,j}$ is the gridbox-specific bias, m and n are the number of grid boxes in longitude (360) and latitude (180) dimension, and w_j is a meridionally varying weighting factor to correct the equal-angle to an equal-area grid (see section 3b). The MB statistic is used in this paper to validate the stability of the global bias.

3) MAB, BIAS CORRECTED, DEFINED GLOBALLY

The global MAB is calculated by first subtracting the global mean bias from every grid box’s bias ($B_{i,j} - \text{MB}$), which

corrects for the general bias. Subsequently, the absolute value is taken from the result, after which a global average is calculated in the same way as done for the global mean bias:

$$\begin{aligned} \text{MAB} &= \frac{1}{mn} \sum_{i=1}^m \sum_{j=1}^n w_j |B_{i,j} - \text{MB}| \\ &= \frac{1}{mn} \sum_{i=1}^m \sum_{j=1}^n w_j |F_{\text{CLARA},i,j} - F_{\text{REF},i,j} - \text{MB}|. \end{aligned} \quad (3)$$

The MAB statistic is used in this paper to validate the processing error (regional uncertainty). Assuming normality, the range between ± 1 MAB contains roughly 57% of the data, and the range between ± 2 MAB contains roughly 89% of the data.

d. Missing data and gap filling

Spatial and temporal gaps in CLARA-A3 are caused by a variety of reasons, discussed extensively in [CM SAF \(2022\)](#) (e.g., missing data in FDR, auxiliary input data). For specific periods, this may significantly impact the calculation of global mean values, leading to unrealistic time series of global mean TOA fluxes. This is avoided by filling these gaps with ERA5 fluxes, which have the advantage of full spatial and temporal coverage. Tests have shown that this gap filling has very little effect on the validation results with bias and MAB (more details in [CM SAF 2022](#)).

e. CLARA-A3 orbital configuration and temporal data visualization

The orbital constellation of AVHRR-carrying satellites is not constant but varies in time regarding the number of satellites, and regarding their respective local equator crossing time (ECT). This is referred to as the “orbital configuration,” which determines the temporal coverage of the observations throughout the day (density and spread of observations) for a given location. A single satellite observes a given location at the equator every 12 h, that is, two times per day (ascending and descending node), from which one during daylight conditions (“daytime”) as illustrated in [Fig. 1](#) (useful for both RSF and OLR), and the other during nighttime, that is, between 1800 and 0600 local time (only useful for OLR).

The satellites are launched on certain typical time slots; historically, these are the morning orbit (around 0730 ECT at launch) and the afternoon orbit (around 1400–1430 ECT at launch). Over time, they each tend to slowly drift toward the terminator, that is, the morning orbit toward an earlier ECT whereas the afternoon orbit toward a later ECT. It is worth mentioning here that this historical configuration was not symmetrical around noon (1200 ECT); that is, the morning orbit is always closer to the terminator relative to the afternoon orbit.

For some periods in the record, there is only one orbit available, either morning or afternoon. This limited temporal coverage is referred to as “suboptimal orbital configuration,” as only a part of the day is covered. Note that it is not a binary issue: even in an orbital configuration with 2 satellites, the temporal coverage can be downgraded when one of the orbits has

strongly drifted toward the terminator, thereby gradually resembling more and more a suboptimal orbital configuration.

The vertical solid gray lines in [Fig. 1](#) indicate transitions (discontinuities) in the orbital configuration, which often correspond to changes in (local) time of observation (i.e., ECT). These lines are included in all of the temporal plots of this paper, and an overview of all these transitions is provided in [Table 1](#).

4. Results for RSF

a. Mean bias and stability

As an illustration, the average CLARA-A3 RSF during 1979–2020 is shown in [Fig. 2](#).

Deseasonalized time series with global monthly mean RSF from different data records are shown in [Fig. 3](#), among which CLARA-A3 RSF in orange (each data record is deseasonalized over its respective full time span). Deseasonalization removes the mean annual cycle and hence also annually recurring biases, which is especially important for ERA5 RSF, as it is characterized by a significant bimodal seasonal bias (largely positive around December, moderately negative and positive around, respectively, April and June, and a largely negative around August; see [CM SAF 2022](#), section 10.3); however, this only works well for systematic seasonal biases (i.e., occurring persistently during every year of the record), which is typically the case for model-based reanalyses such as ERA5. The deseasonalized ERA5 time series proves to be stable and can be used to assess the stability of other data records in the pre-CERES era (1979–99). The two major volcanic eruptions El Chichón and Pinatubo are indicated on the time series, both having a radiative impact duration of about 21 months. El Chichón’s radiative impact is estimated at +3 (CLARA-A3) and +2 (ERA5) W m^{-2} , while Pinatubo’s impact is estimated at +5 (CLARA-A3), +4 (ERA5), and +6 (ISCCP-FH) W m^{-2} . The volcanic eruptions led to a dramatic increase in stratospheric sulfate aerosol loading, causing a large rise in the reflection of solar radiation due to the optical properties of sulfuric acid droplets ([Canty et al. 2013](#)). Unlike the Pinatubo event, CLARA-A3 RSF does not properly capture the radiative impact of the El Chichón event: it features a temporary artificial drop of $\sim 2 \text{ W m}^{-2}$ with respect to ERA5 during the event, around January 1983 ([Fig. 3](#)).

Global mean biases are calculated by subtracting the reference data records from CLARA-A3 RSF, resulting in the time series shown in [Fig. 4](#) (deseasonalization is performed over the overlapping period of both data records, after they have been subtracted from each other). The overall stability of CLARA-A3 RSF is assessed with respect to ERA5 ([section 2e](#)) by considering a so-called “stability envelope” (target range), set symmetrically around the (slightly negative) mean of the bias, which is normally distributed ([CM SAF 2022](#), section 5.1). The threshold requirement of 4 W m^{-2} cited in [CM SAF \(2021, 62–63\)](#) is selected as range for this envelope, and the overall stability remains within its limits for 94% of the time. During the CERES era (2000–20) the CLARA-A3 RSF performance is very good, with a mean bias with respect to CERES SYN close to zero for the larger part of the two decades

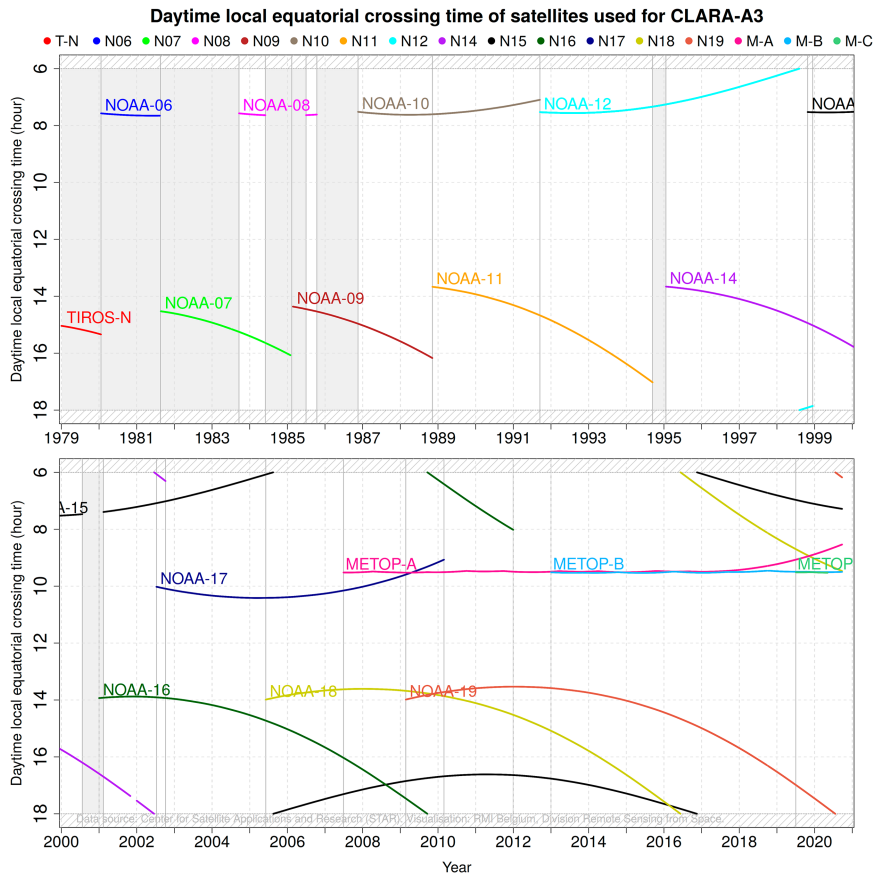


FIG. 1. Daytime local equator crossing time of satellites used for CLARA-A3. Gray-shaded areas indicate suboptimal time periods, and hatched areas indicate nighttime.

(red curve in Fig. 4). The largest bias fluctuations are situated in the first decade of the data record (until 1987), where the monthly RSF bias with respect to ERA5 (black curve) approaches or exceeds the edges of the stability envelope, but there are also some isolated peaks in later years (1994–95, 1999, and 2000). These biases are predominantly caused by CLARA-A3’s “suboptimal orbital configuration” (section 3e): Incomplete temporal coverage of regional climate phenomena with an asymmetric diurnal cycle (e.g., marine stratocumulus thinning, land convection) introduces strong regional biases, from which the sign (positive or negative) depends on the region and observation time (morning, afternoon). Globally averaged, these biases vary seasonally because of the hemispherical imbalance of the associated regional climate feature’s occurrence and strength. As a result, it introduces a seasonally varying global mean bias during years with suboptimal orbital configuration (Table 1), which, in contrast to ERA5 biases, is not removed after deseasonalization, given its limited time span with respect to the entire data record’s duration. The suboptimal configuration with only afternoon satellites (Table 1) is characterized by a unimodal seasonal bias (negative between November and February and positive between April and July), which causes the CLARA-A3 RSF radiative effect of the El Chichón event to be not well

represented (cf. the drop in CLARA-A3 RSF of about $\sim 2 \text{ W m}^{-2}$ with respect to ERA5 around January 1983 in Figs. 3 and 4).

In the period of the Pinatubo eruption, between April 1991 and January 1993 (Figs. 3 and 4), the bias between CLARA-A3 RSF and ERA5 increases by more than $+1 \text{ W m}^{-2}$ relative to the period before and after. Here it probably concerns a bias in the ERA5 reanalyses, in which an underestimation of the prescribed aerosol optical depth would explain an underestimated RSF.

A slight downward trend in CLARA-A3 RSF of about -1 W m^{-2} can be noticed between 2015 and 2020, which is caused by a trend in one of the satellites’ level-1 data record (*MetOp-B*) (as demonstrated in CM SAF 2022, section 11.3.3). Note that *MetOp-B* was not well characterized because of its limited historic record when the FDR was generated (Karlsson et al. 2023b). At that time, it was difficult to predict such a degradation and anticipate its future calibration parameters.

In absolute terms, it is not surprising that CLARA-A3 is close to CERES-SYN1deg (red curve in Fig. 4) given the empirical relations between AVHRR and CERES that were first established offline (Akkermans and Clerbaux 2020) and then used to derive CERES-like broadband quantities in the data

TABLE 1. Transitions in CLARA-A3 orbital configuration; abbreviations: T-N is TIROS-N, N-X is NOAA-X, aft is afternoon, mor is morning, and subopt is suboptimal). Boldface type indicates periods with suboptimal orbital configuration.

Date (start)	Date (end)	Satellite(s)	Orbital configuration
1 Jan 1979	20 Jan 1980	T-N	Aft (=subopt)
20 Jan 1980	19 Aug 1981	N-6	Mor (=subopt)
19 Aug 1981	19 Sep 1983	N-7	Aft (=subopt)
19 Sep 1983	1 Jun 1984	N-8; N-7	Mor; aft
1 Jun 1984	13 Feb 1985	N-7	Aft (=subopt)
13 Feb 1985	1 Jul 1985	N-9	Aft (=subopt)
1 Jul 1985	14 Oct 1985	N-8; N-9	Mor; aft
14 Oct 1985	17 Nov 1986	N-9	Aft (=subopt)
17 Nov 1986	8 Nov 1988	N-10; N-9	Mor; aft
8 Nov 1988	16 Sep 1991	N-10; N-11	Mor; aft
16 Sep 1991	13 Sep 1994	N-12; N-11	Mor; aft
13 Sep 1994	20 Jan 1995	N-12	Mor (=subopt)
20 Jan 1995	26 Oct 1998	N-12; N-14	Mor; aft
26 Oct 1998	14 Dec 1998	N-15; N-14; N-12	Mor; aft
14 Dec 1998	22 Jul 2000	N-15; N-14	Mor; aft
22 Jul 2000	1 Jan 2001	N-14	Late aft (=subopt)
1 Jan 2001	12 Feb 2001	N-16; N-14	Aft (=subopt)
12 Feb 2001	11 Jul 2002	N-15; N-16; N-14	Mor; aft
11 Jul 2002	31 Dec 2020	(Multiple)	Mor; midmor; aft

record’s processing (Akkermans and Clerbaux 2021): this could be considered a kind of “tuning” or “recalibration” of the absolute radiometric level. More importantly, this time series is relatively flat, which indicates a good stability with respect to the CERES products. The bias with CERES-EBAF is consistently $\sim 1.5 \text{ W m}^{-2}$ lower (green curve in Fig. 4), which can be explained by the EBAF adjustments made to comply with current estimates of the global energy imbalance. Similar to CLARA-A3 RSF, the Cloud-CCI data record is based on the AVHRR instrument, but the Cloud-CCI product shown in Fig. 4 (in gray) is only based on afternoon satellites. Its overall stability is reasonable, mostly hovering from -2 to -3 W m^{-2} with respect to CERES-SYN and CLARA-A3. The

ISCCP-FH data record is considered the least performing, given its seemingly random and large short-term fluctuations (on the order of $2\text{--}3 \text{ W m}^{-2}$) as well as long-term instability (oscillating between -10 and -5 W m^{-2} with respect to CERES-SYN and CLARA-A3).

The daily mean analysis is not shown here, because the biases’ magnitude and fluctuations are similar and are not affected by the temporal aggregation.

b. Processing error (regional uncertainty)

First the CERES era is discussed, that is, the years 2000–20 (Fig. 5). The months August 2000, June 2001, and March 2002 are not validated since the CERES products contain data

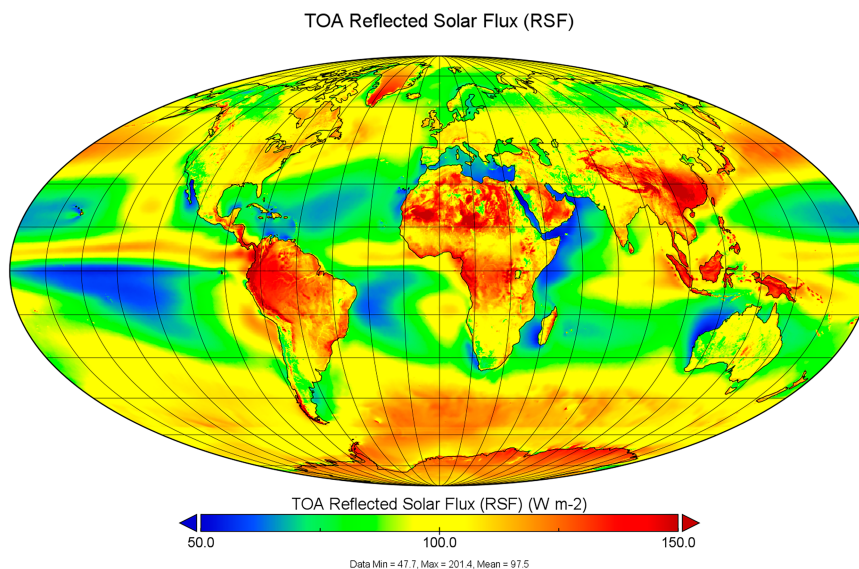


FIG. 2. Average CLARA-A3 RSF during 1979–2020.

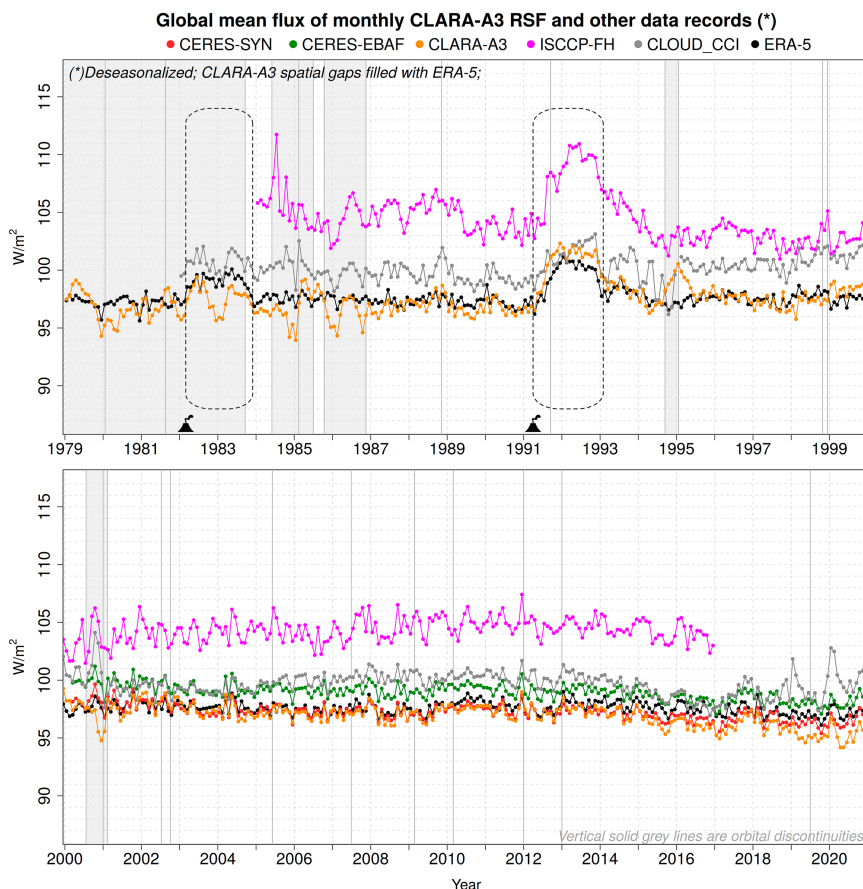


FIG. 3. Deseasonalized global mean flux of monthly CLARA-A3 RSF (in orange) and other data records.

gaps in those months, resulting in a total number of 247 months.

On average, the monthly MAB (with respect to CERES SYN1deg-month) amounts 2.3 W m^{-2} and the daily MAB (with respect to CERES SYN1deg-day) amounts 6.2 W m^{-2} (red curves in Fig. 5). Much more than for the mean bias (section 4a), the processing error (regional uncertainty) during the CERES era is clearly related to the orbital configuration (Fig. 1). Best performance, with monthly and daily MAB around 2 and 5 W m^{-2} , respectively, is obtained with a maximum number and best spread of satellite observations throughout the day, that is, best temporal coverage (2002–16). The gradual decrease in performance (i.e., increase of MAB) after 2016 is due to orbital drift of the afternoon satellite toward an evening orbit (without introducing a new afternoon orbit with AVHRR instrument). The first years, until mid-2002, are characterized by a markedly higher monthly and daily MAB, and again the main reason is the orbital configuration: indeed, the midmorning orbit is only available since mid-2002. The sharp peak during the second half of 2000 represents the worst orbital configuration, being a single late afternoon orbit. The following distinct periods during the CERES era can be delineated, with MAB exhibiting large

fluctuations with sharp delineations that are relatable to orbital configuration changes:

- 1) first half of 2000 with morning + late afternoon satellite: Monthly and daily MAB of 4 and $10\text{--}13 \text{ W m}^{-2}$, respectively,
- 2) second half of 2000 with a single late afternoon satellite (NOAA-14): Monthly and daily MAB of 6–8 and $19\text{--}21 \text{ W m}^{-2}$, respectively,
- 3) between 2001 and mid-2002 with morning + afternoon satellite: Monthly and daily MAB of 2.5–3.5 and $8\text{--}10 \text{ W m}^{-2}$, respectively,
- 4) between mid-2002 and 2016 with midmorning (NOAA-17) + afternoon satellite: Monthly and daily MAB of 2 and 5 W m^{-2} , respectively, and
- 5) after 2016 with midmorning and drifting afternoon satellite (NOAA-19): Monthly MAB gradually increasing from 2 to 4 W m^{-2} (monthly) and from 5 to 10 W m^{-2} (daily).

A consistent seasonal cycle of the monthly MAB with respect to CERES EBAF is noticeable (green curve in Fig. 5), contrary to the absence of such pattern in the MAB with respect to CERES SYN1deg (red curve), a discrepancy that is probably caused by a difference in the processing of CERES

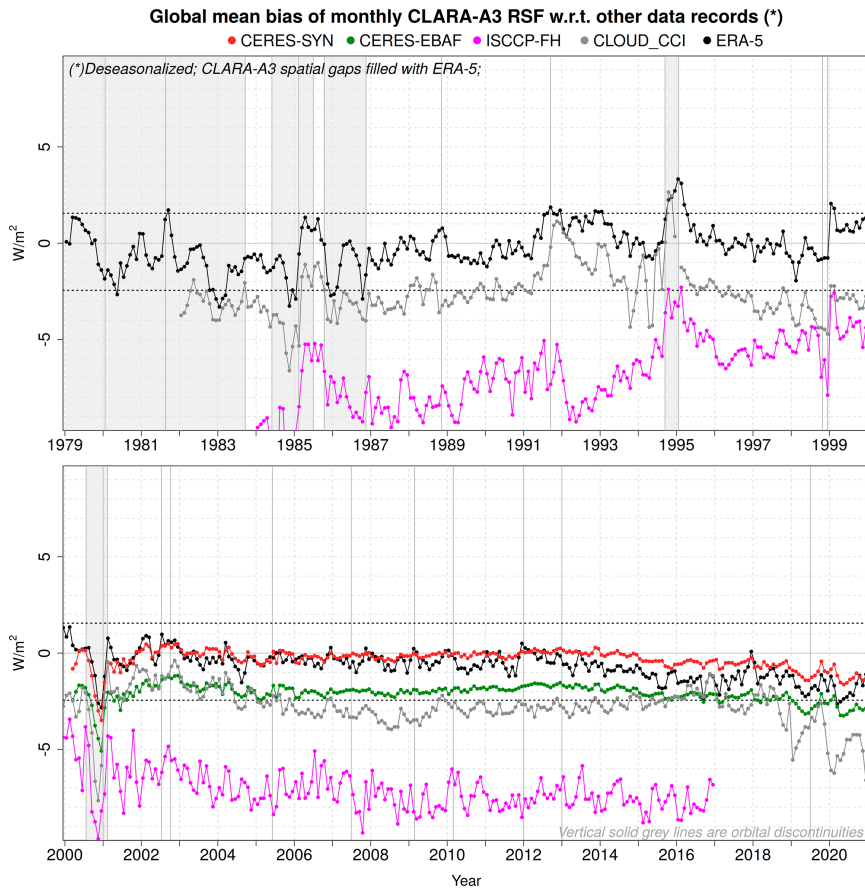


FIG. 4. Deseasonalized global mean bias of monthly CLARA-A3 RSF with respect to other data records. Dotted lines indicate a stability envelope of 4 W m^{-2} around the bias with respect to ERA5.

products. However, the latter is not entirely free from seasonality: the first and last few years of the MAB with respect to SYN1deg are also characterized by an increased seasonality (especially in the daily MAB), which is related to the

abovementioned *NOAA-19*'s orbital drift and the absence of *NOAA-17*'s midmorning orbit.

The increased MAB as well as its gradually increasing seasonality can both be explained by a degrading temporal coverage

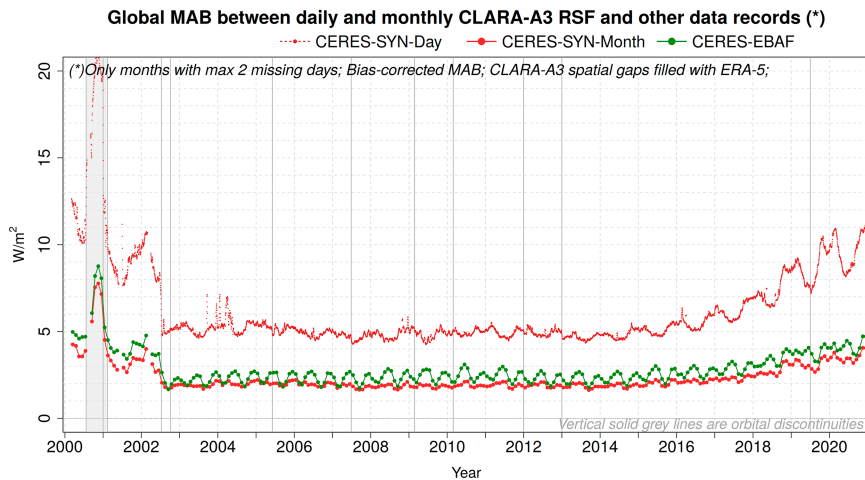


FIG. 5. Global MAB between daily and monthly CLARA-A3 RSF and other data records. Daily MAB is systematically higher than monthly MAB.

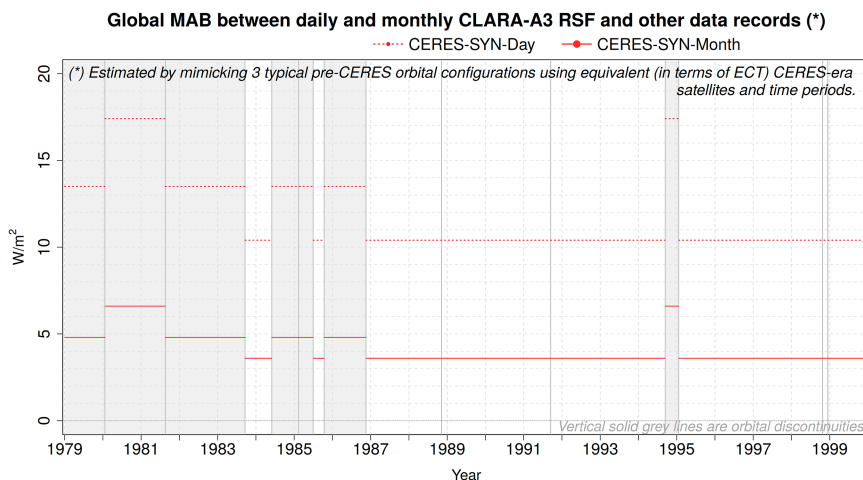


FIG. 6. Global MAB between daily and monthly CLARA-A3 RSF and the CERES-SYN data records, estimated by mimicking three typical pre-CERES orbital configurations using equivalent (in terms of ECT) CERES-era satellites and time periods.

over regions characterized by large-scale regional climate phenomena with an asymmetric diurnal cycle (e.g., marine stratus thinning or land convection). This introduces strong regional biases, which can be positive or negative, depending on the region and kind of phenomena. Furthermore, a degrading temporal coverage also introduces strong biases with fast moving small-scale or heterogeneous weather systems (e.g., fronts), typically consisting of swirls with positive alongside negative bias, caused by an extrapolation of, for example, the midmorning observation to the afternoon (when the afternoon satellite has disappeared or drifted toward the evening), or simply put: the weather moves too fast to be accurately observed (Akkermans and Clerbaux 2021). Globally averaged together, all these biases vary seasonally because of a hemispherical imbalance of the associated regional climate features' occurrence and strength, explaining the seasonal pattern of MAB. With any degradation of the temporal coverage (orbital configuration), such as *NOAA-19*'s orbital drift, these regional biases grow accordingly, thereby directly increasing the global MAB (Fig. 5). In contrast, the global mean bias is much less sensitive and remains relatively stable and without seasonal pattern during the CERES era (cf. red curve in Fig. 4) because of compensating negative and positive regional biases. The bias is only affected with much worse temporal coverage, prevailing mainly during the pre-CERES era (suboptimal orbital configuration).

In addition, we mention that observations with low illumination conditions (high solar zenith angle), prevalent close to the terminator, lead to a larger processing error, for instance, due to the increased uncertainty of scene type defining parameters (cloud mask, cloud optical thickness, cloud phase, etc.), that propagates as uncertainty in the narrowband-to-broadband and ADM processes. This effect is also tied to the orbital configuration, as orbital drift typically increases the average solar zenith angle for a given location.

Besides the common overall characteristics and features of daily and monthly MAB, the daily MAB is generally higher

than the monthly MAB. The reason is bias compensation, on different levels and scales. First, there is a temporal sampling compensation: biases caused by fast moving small-scale or heterogeneous weather systems (e.g., broken cloud fields) vary in sign from day to day, depending on the weather system's morphology and movements (direction, timing, speed, etc.). The aggregation to a monthly mean bias smooths out this daily variability. Second, there are numerous error sources related to the retrieval of instantaneous TOA albedo, which are propagated to the daily mean RSF (and the less satellite observations per day, the stronger this propagation). However, averaged over 30 days many of these errors tend to cancel each other out. Examples are the errors related to the ADM (viewing and illumination geometry change every day, this in contrast to geostationary observations) and errors related to scene type identification such as cloud cover and cloud properties (relevant for ADM but also for narrowband-to-broadband conversion, etc.). According to the terminology outlined in section 3a, these kinds of compensating errors could for a large part be considered as the random component of the processing error ("precision part"), characterized by the daily MAB, whereas the errors that are still detected in the monthly MAB could be considered the processing error's systematic component ("accuracy part").

Until here the MAB validation only concerns the so-called CERES era (2000–20), roughly corresponding to the second half of CLARA-A3's data record time span. The first half of the record does not have a suitable reference data record to estimate the regional uncertainty. However, since it is clear from the second half of the record that the orbital configuration explains most of the variability, it is possible to estimate the MAB during the pre-CERES era by mimicking three typical pre-CERES orbital configurations using equivalent (in terms of ECT) CERES-era satellites and time periods. The appendix provides the details of this theoretical exercise, from which the results can be viewed in Fig. 6 (years 1979–99).

TOA outgoing longwave radiation (OLR)

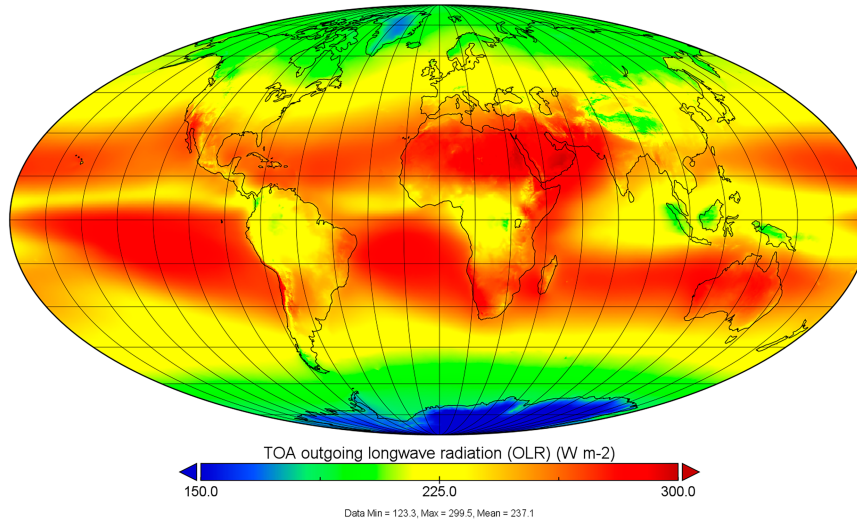


FIG. 7. Average CLARA-A3 OLR during 1979–2020.

Daily MAB for the morning-only orbital configuration is estimated at 17.4 W m^{-2} , whereas the afternoon-only configuration at only 13.5 W m^{-2} . This difference is due to their temporal asymmetry around solar noon, that is, the morning orbit being closer to the morning terminator than the afternoon orbit is from the evening terminator (see section 3e). The result is that for the entire data record time span, the average monthly and daily MAB with respect to CERES-SYN1deg is estimated at 3.2 and 9.0 W m^{-2} , respectively.

5. Results for OLR

a. Mean bias and stability

The average CLARA-A3 OLR during 1979–2020 is shown in Fig. 7.

The deseasonalized global monthly mean OLR from different data records is shown in Fig. 8, among which CLARA-A3 OLR in orange. The HIRS and ERA5 data records are stable with respect to each other, increasing the confidence in their ability to serve as stability benchmark for the other data records. Volcanically induced aerosols also trap thermal radiation, but the longwave radiative impact is lower than that of the shortwave (Canty et al. 2013), shown in section 4a, so that the net effect is a climate cooling. The two major volcanic eruptions El Chichón and Pinatubo are indicated on the time series in Fig. 8. The El Chichón eruption has no clear impact in the CLARA-A3 data record (but it might have caused a small drop of -0.5 W m^{-2} in other data records), whereas the Pinatubo event probably caused a drop in OLR of approximately -1 W m^{-2} , which is about one-half of the assumed impact as seen in the HIRS OLR data records (-2 W m^{-2}). This volcanic forcing is predominantly caused by a direct aerosol–radiation effect, but to a smaller extent also affected by indirect aerosol–cloud effects such as changes in cirrus cloud properties (Schmidt et al. 2018). Overall, for most data records these radiative impacts are almost similar to many

other drops and jumps in the time series, making it difficult to assess and quantify them.

The global mean bias is calculated by subtracting the reference data records from CLARA-A3 OLR, resulting in the time series shown in Fig. 9. The overall stability of CLARA-A3 OLR is assessed with respect to HIRS (section 2c), and similar to the RSF validation, this is done using a stability envelope with a range of 4 W m^{-2} (i.e., the threshold requirement cited in CM SAF 2021, 62–63), which is arbitrarily set to $[-3.2; +0.8] \text{ W m}^{-2}$ because the OLR bias is not normally distributed (figure not shown), as explained in CM SAF (2022, section 6.1). The overall stability remains within its limits for 99.6% of the time. The same results are obtained when assessing the stability with respect to HIRS-MM (section 2d). During the CERES era (2000–20) the CLARA-A3 OLR performance is very good, with a relatively “flat” mean bias with respect to CERES SYN, with an MAB between -1 and 0 W m^{-2} for the larger part of the two decades. Note that CERES-EBAF is consistently $\sim 1.5 \text{ W m}^{-2}$ lower (green curve in Fig. 9), which is explained by the EBAF adjustments made to comply with current estimates of the global energy imbalance.

The first few years of the records are characterized by a distinctively more negative mean bias in comparison with the rest of the record. This period corresponds to coverage from the TIROS-N and NOAA-6 satellites (January 1979–August 1981) and has an average bias of -2.5 W m^{-2} , which is markedly lower than the mean bias between 1982 and 2002 (around -1 W m^{-2}) and between 2002 and 2020 (around 0 W m^{-2}). Additional investigations (analyses and figures not shown) exclude some potential factors as main cause (e.g., the morning-only orbital configuration, or the fact that early AVHRR instruments have only one thermal infrared channel) and indicate that the bias is likely due to an issue either with the calibration of the FDR or with the spectral response correction factors. The remaining first half of the record

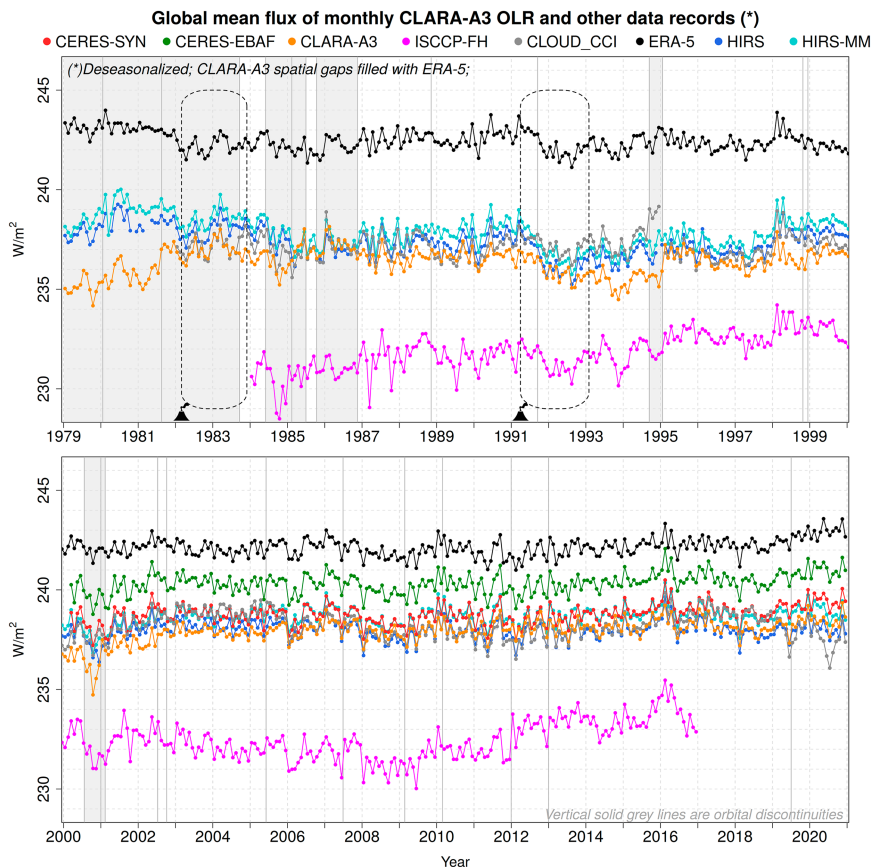


FIG. 8. Deseasonalized global mean flux of monthly CLARA-A3 OLR (in orange) and other data records.

(1981–99) is characterized by subtle patterns related to orbital configuration, most notably the gradual shift toward more negative biases with increasing ECT (orbital drift) marking distinct periods being 1985–89, 1989–94, and 1994–99.

The daily mean analysis is not shown here, because the biases' magnitude and fluctuations are similar to the monthly results.

b. Processing error (regional uncertainty)

On average, the monthly and daily MAB with respect to HIRS (Fig. 10) amounts 1.8 and 4.8 W m^{-2} , respectively. The daily MAB exhibits significant fluctuations with clear delineations that are relatable to changes in orbital configuration:

- 1) between 1979–mid-1983 and mid-1984–86 with suboptimal orbital configurations, that is, morning-only or afternoon-only satellite: daily MAB of 6–8 W m^{-2} ,
- 2) the first half of 1984 and between 1987 and 2002, with mostly morning + afternoon satellites: daily MAB of 4–6 W m^{-2} , slightly varying according to orbital drift,
- 3) distinct peaks during 1995 and 2000, with, respectively, an only-early-morning and an only-late-afternoon satellite: daily MAB of around 8 W m^{-2} ,
- 4) between 2002 and 2016 with midmorning + afternoon satellites: daily MAB of 3.7 W m^{-2} , and

- 5) after 2016 with midmorning + drifting afternoon satellite: daily MAB increasing to 4.5 W m^{-2} .

Between April and October 1985 there are no valid HIRS observations, explaining the data gap in this period.

The underlying reasons for the dependency of OLR MAB on the orbital configuration are identical to the ones for RSF, as described in section 4b; however, the OLR is much less sensitive to it (cf. Figs. 5 and 10): the absence of the midmorning orbit *NOAA-17* (before mid-2002) and the orbital drift of the afternoon orbit *NOAA-19* (after 2016) both have only a small impact on OLR's daily MAB (+0.5 to +1.0 W m^{-2}), which is quasi constant between 2002 and 2016 (around 3.7 W m^{-2}). Large degradations in orbital configurations have a bigger impact, for instance, the late-afternoon-only configuration in the second half of 2000, causing the MAB to double (to 8 W m^{-2}); however, these impacts are still small relative to RSF, where the same degradation leads to a quadrupling of MAB (Fig. 5). There are multiple reasons for this, for instance, the intraday relative range, which is much lower for OLR than for RSF, thereby lowering the impact of wrong temporal extrapolation due to suboptimal temporal coverage. Another reason is the number of observations per day, which for OLR is double (relative to RSF) because it also relies on nighttime observations,

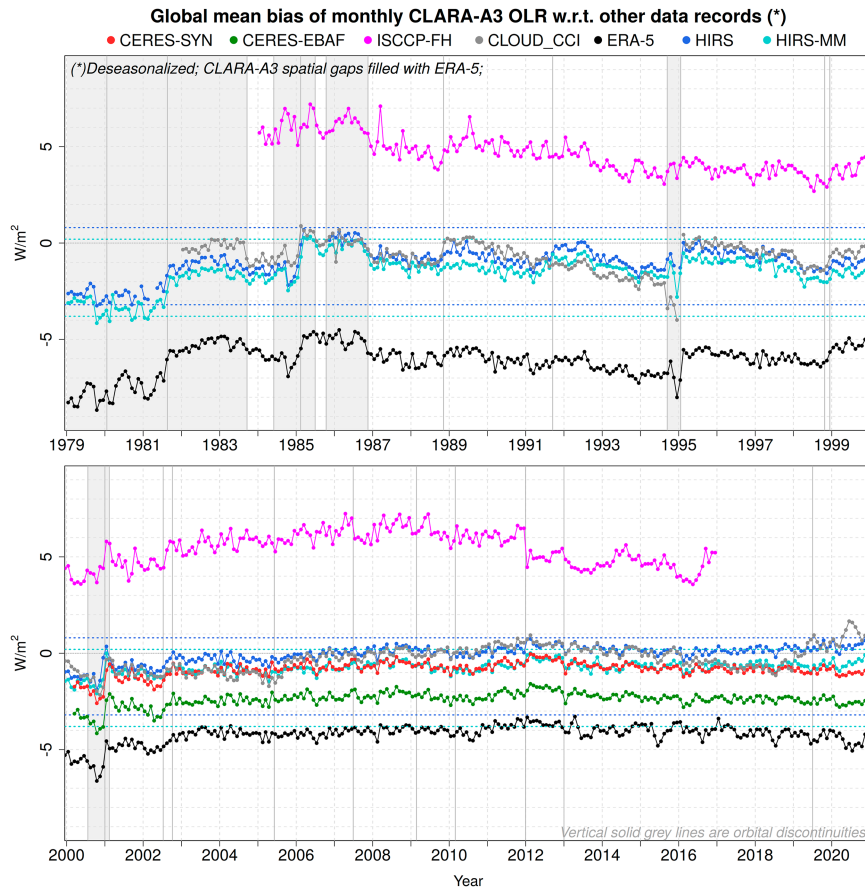


FIG. 9. Deseasonalized global mean bias of monthly CLARA-A3 OLR with respect to other data records. Dotted lines indicate a stability envelope of 4 W m^{-2} around the bias with respect to HIRS.

which again lowers the impact of suboptimal temporal coverage on the daily mean integration.

In contrast to the daily MAB, the monthly MAB is even less sensitive to orbital configuration, for the same reasons as outlined in section 4b. It has a quasi-constant MAB of around 1.5 W m^{-2} between 2001 and 2020 (barely impacted by *NOAA-19*'s orbital drift and absence of *NOAA-17*'s midmorning orbit). On the other hand, large degradations in orbital configurations do have an impact, for instance, the late-afternoon-only configuration in the second half of 2000, causing the MAB to increase to $2.5\text{--}3.0 \text{ W m}^{-2}$; also here, these impacts are still small relative to the RSF, where the same degradation leads to a quadrupling of monthly MAB (Fig. 5).

6. Regional comparison (geographical distribution)

Although a regional analysis of the bias is beyond the scope of this paper, a bias map should provide basic confidence in its spatial distribution, for instance, to verify that there are no problematic spatial differences. The 2000–20 multiannual mean of CLARA-A3 RSF bias with respect to CERES-SYN1deg is shown in Fig. 11. The biases are generally relatively low in most regions (within $\pm 2 \text{ W m}^{-2}$), with some regions showing

systematically (slightly) larger biases, in both negative sense (darker bluish colors; e.g., ocean west of African continent, Antarctica, eastern Canada) and positive sense (darker reddish colors; e.g., nondesert African and Southeast Asian landmasses), possibly related to specific scene types (snow/ice, tropical forest). Overall, however, the long-term averaged bias is considered acceptably low and sufficiently homogeneous.

The 1979–2020 multiannual mean of CLARA-A3 OLR bias with respect to HIRS OLR is shown in Fig. 12. The biases are generally relatively low in most regions (within $\pm 2 \text{ W m}^{-2}$), with almost no region-specific bias. Also here, the long-term averaged bias is considered acceptably low and sufficiently homogeneous. The HIRS and AVHRR instruments are on the same satellite, which is partly the reason for these low regional biases (in comparison with the RSF bias map).

7. Conclusions

This paper provides a first validation of the new CLARA-A3 TOA flux products, RSF and OLR, on their full temporal extent.

The CLARA-A3 reflected solar flux data record is relatively stable as its bias with respect to ERA5 remains within $\pm 2 \text{ W m}^{-2}$ for 94% of the time. Deviations are predominantly

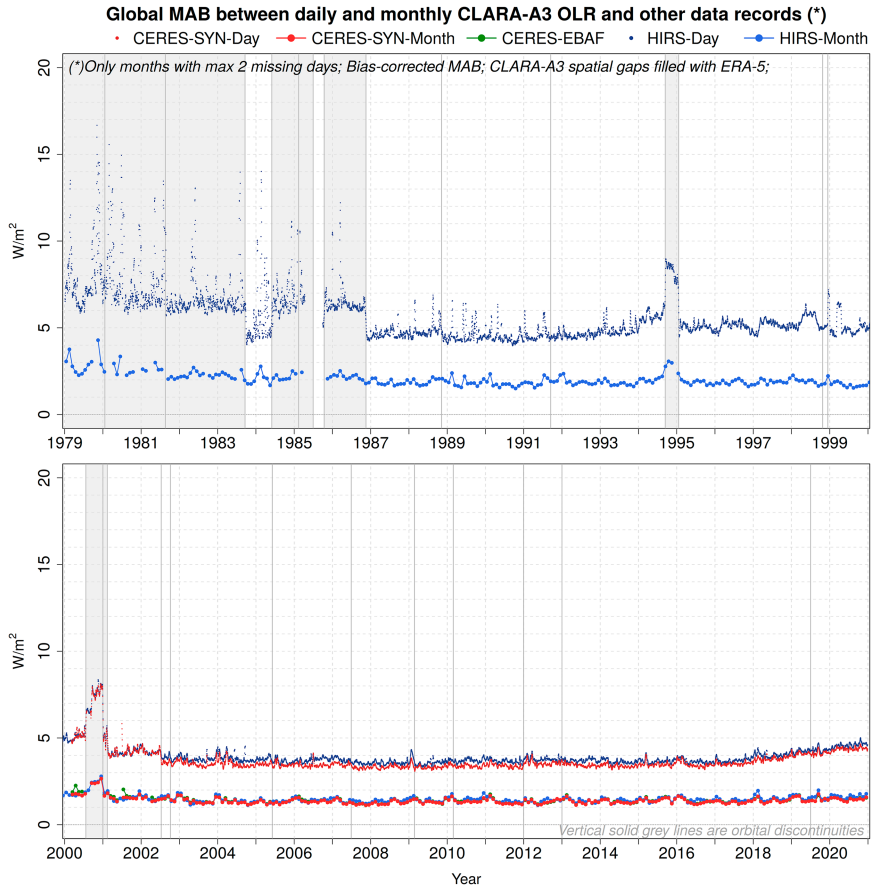


FIG. 10. Global MAB between daily and monthly CLARA-A3 OLR and other data records. Daily MAB is systematically 2–3 $W m^{-2}$ higher than monthly MAB.

caused by incomplete temporal coverage (only morning or only afternoon orbit), which occurs mostly in the first decade of the record. The radiative impact of the Pinatubo volcanic eruption is estimated at $3 W m^{-2}$. The RSF processing error

(regional uncertainty) correlates with orbital configuration: Best performance, around $2 W m^{-2}$ for monthly MAB, is found with highest temporal coverage, that is, number of contributing satellite orbits and spread in their overpass time,

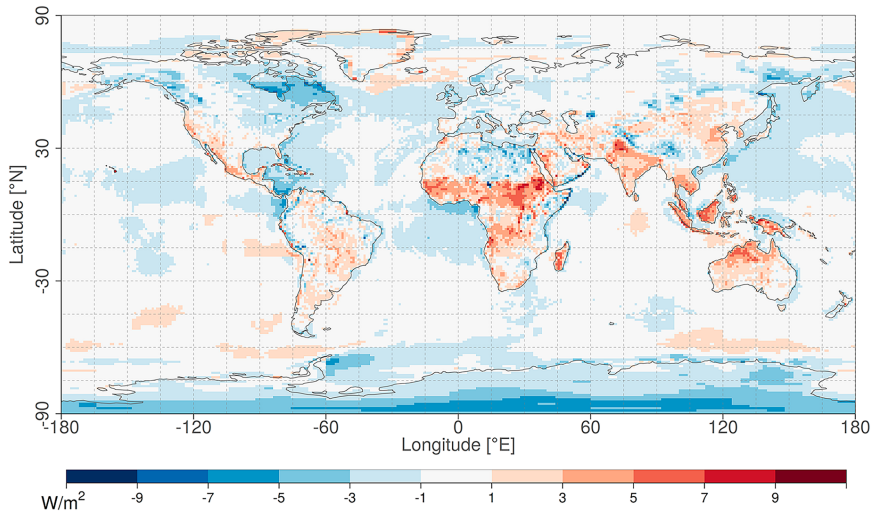


FIG. 11. Average RSF bias during 2000–20 between CLARA-A3 and CERES-SYN1deg.

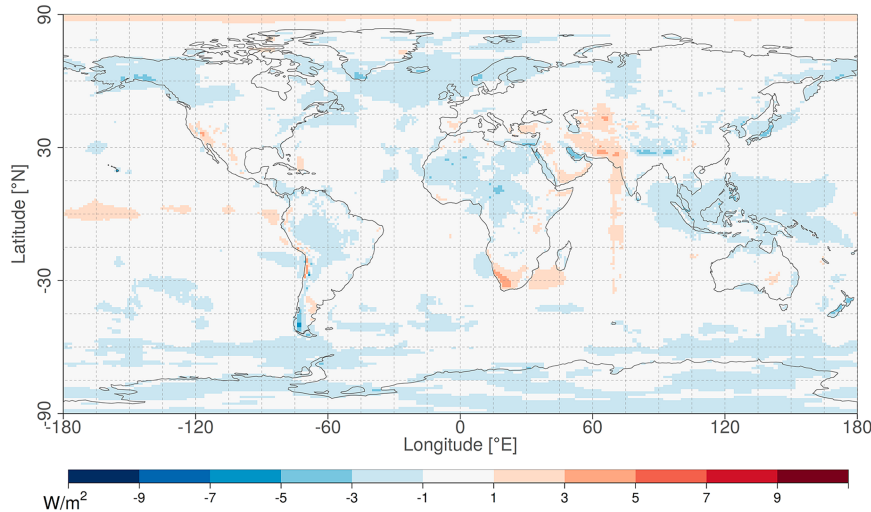


FIG. 12. Average OLR bias during 1979–2020 between CLARA-A3 and HIRS-OLR.

which is optimal during 2002–16. Absence of the midmorning orbit (before 2002) or early afternoon orbit (gradually after 2016) leads to a drop in performance (doubling of MAB).

The CLARA-A3 outgoing longwave radiation data record is found relatively stable with respect to both ERA5 and the HIRS OLR data records, except for the first two years. Furthermore, orbital drift has a noticeable effect on the bias during the first half of the record (1979–99). The OLR processing error is less sensitive to orbital configuration when compared with RSF, but especially for the daily MAB there is still a significantly lower performance (MAB +40%) for morning-only and afternoon-only orbits (1979–87).

Overall, these validation results are satisfactory for the first edition of the flux products in the CLARA-A product portfolio. Uncertainties inherent to the polar orbiting satellite constellation are difficult to correct, especially for a constellation with persisting orbital drift, as is the case with most NOAA satellites; this is in contrast to the CERES products, where the constant local observation time (equatorial overpass time) of the *Aqua* and *Terra* satellites allows for the development and implementation of a fixed instantaneous-to-diurnal correction. However, some potential improvements for future editions can be noted: 1) Updating the currently implemented CERES Ed2 ADMs to the newest available CERES Ed4 ADMs could improve the instantaneous RSF estimation, as well as the albedo diurnal cycle models used to derive the daily mean flux. 2) The effects of the last afternoon orbit's disappearance (*NOAA-19*) due to orbital drift could be solved by introducing the VIIRS instrument on board satellites with an afternoon orbit, alongside the existing AVHRR-carrying satellites. 3) An update of the FDR with the newest calibration coefficients could solve calibration issues with the most recent satellites, such as *MetOp-B* and *MetOp-C* (and possibly also the two oldest, *TIROS-N* and *NOAA-6*). 4) Improving and tuning of AVHRR-derived geophysical parameters (such as cloud optical thickness) to better mimic the original CERES/MODIS-derived parameters (that were used to construct the CERES ADM's), thereby decreasing the uncertainty

and/or bias associated with scene type identification needed for ADM selection.

The CLARA-A3 RSF and OLR products have unique properties, such as an unprecedented high resolution of 0.25° and almost double the time span of the current CERES data records. Another advantage is the flux product's synergy and compatibility with the other CLARA-A3 CDRs (cloud mask and other cloud parameters, surface radiation, surface albedo, etc.) sharing common algorithms and processing chains.

Acknowledgments. This work was funded by the Climate Monitoring Satellite Application Facility (CM SAF) of EUMETSAT. The authors are grateful to the Atmospheric Science Data Center at NASA Langley Research Center for providing the CERES data used in this work. The ERA5 data have been obtained from the Copernicus Climate Data Store (CDS).

Data availability statement. The CLARA-A3 documentation consists of an algorithm theoretical basis document (ATBD), validation report (VAL), and product user manual (PUM), all available online (https://doi.org/10.5676/EUM_SAF_CM/CLARA_AVHRR/V003, which also contains hyperlinks to the CM SAF web user interface, where the actual data can be freely downloaded).

APPENDIX

RSF Processing Error (Regional Uncertainty) during the Pre-Ceres Era (1979–99)

Three typical orbital configurations (defining observational temporal coverage of the diurnal cycle) exist in the pre-CERES (1979–99) period of the data record: morning only, afternoon only, and morning + afternoon. Each of these three configurations is mimicked using a selection of CERES-era satellites that are equivalent in terms of ECT during limited time periods,

TABLE A1. Estimation of RSF uncertainty during pre-CERES era; T is TIROS, N is NOAA, and ECT is equator crossing time. Means are boldfaced for ease of reference.

Orbital configuration	Pre-CERES (1979–99) orbital configuration			CERES-era (2000–20) equivalent orbital configuration (similar local ECT)		
	Satellite	Duration (months)	Satellite	Duration	Monthly MAB ($W m^{-2}$)	Daily MAB ($W m^{-2}$)
I: Afternoon satellite only	T-N	Jan 1979–Jan 1980: 13	N-16	Jan 2005–Dec 2006	Range: 4.1–6.3	Range: 10.6–19.1
	N-7	Sep 1981–Aug 1983: 24	N-18	Jan 2012–Dec 2013	Mean: 4.8	Mean: 13.5
	N-7	Jun 1984–Jan 1985: 8	N-19	Jan 2016–Dec 2017	<8 (100%)	<16 (88.7%)
	N-9	Feb–Jun 1985: 5			<4 (0%)	<8 (0%)
	N-9	Nov 1985–Oct 1986: 12			<2 (0%)	<4 (0%)
		Total: 62 months				
II: Morning satellite only	N-6	Feb 1980–Aug 1981: 19	N-15	Mar–Jul 2000	Range: 5.2–8.6	Range: 13.2–23.1
	N-12	Sep–Dec 1994: 4	N-15	Mar–Jun 2001	Mean: 6.6	Mean: 17.4
		Total: 23 months	N-16	Jan–Dec 2011	<8 (84.8%)	<16 (35.3%)
			N-18	Jul 2017–Jun 2018	<4 (0%)	<8 (0%)
					<2 (0%)	<4 (0%)
III: Afternoon and morning satellite only	N-7/ N-8	Sep 1983–May 1984: 9	N-14/N-15	March–July 2001	Range: 2.3–6.3	Range: 6.7–19.0
	N-9/ N-8	Jul–Oct 1985: 4	N-15/ N-16	January 2004–December 2005	Mean: 3.6	Mean: 10.4
	N-9/ N-10	Nov 1986–Oct 1988: 24	N-16/ N-18	January–December 2011	<8 (100%)	<16 (99.2%)
	N-11/ N-10	Nov 1988–Sep 1991: 35	N-18/ N-19	July 2017–June 2018	<4 (73.6%)	<8 (15.7%)
	N-11/ N-12	Oct 1991–Aug 1994: 35			<2 (0%)	<4 (0%)
	N-14/ N-12	Jan 1995–Nov 1998: 47				
	N-14/ N-15	Dec 1998–Feb 2000: 15				
	Total: 169 months					

an overview of which is provided in Table A1 (e.g., morning satellites mimicked by *NOAA-16* or *NOAA-18*, when they drifted to 0700–0800 local time).

Subsequently, daily and monthly mean RSF data are generated for each of the three typical orbital configurations, each using its own associated selection of (CERES-era) satellites and limited time periods. From this, the average processing error (MAB) for each typical orbital configuration is calculated (last two columns in Table A1). Since we know the orbital configuration is the largest source of error, these numbers provide an estimate of the processing error during the pre-CERES era.

Hence, it is now possible to “fill” the gap in the entire data record’s processing error time series, that is, extending Fig. 5 back in time, resulting in Fig. 6.

REFERENCES

- Akkermans, T., and N. Clerbaux, 2020: Narrowband-to-broadband conversions for top-of-atmosphere reflectance from the Advanced Very High Resolution Radiometer (AVHRR). *Remote Sens.*, **12**, 305, <https://doi.org/10.3390/rs12020305>.
- , and —, 2021: Retrieval of daily mean top-of-atmosphere reflected solar flux using the Advanced Very High Resolution Radiometer (AVHRR) instruments. *Remote Sens.*, **13**, 3695, <https://doi.org/10.3390/rs13183695>.
- Canty, T., N. R. Mascioli, M. D. Smarte, and R. J. Salawitch, 2013: An empirical model of global climate—Part 1: A critical evaluation of volcanic cooling. *Atmos. Chem. Phys.*, **13**, 3997–4031, <https://doi.org/10.5194/acp-13-3997-2013>.
- Clerbaux, N., T. Akkermans, E. Baudrez, A. Velazquez Blazquez, W. Moutier, J. Moreels, and C. Aebi, 2020: The Climate Monitoring SAF outgoing longwave radiation from AVHRR. *Remote Sens.*, **12**, 929, <https://doi.org/10.3390/rs12060929>.
- CM SAF, 2021: CDOP-3 product requirements document. CM SAF Doc. SAF/CM/DWD/PRD v3.8, 170 pp.
- , 2022: Validation report for top-of-atmosphere products from the CMSAF cloud, albedo, radiation data record, AVHRR-based, Edition 3 (CLARA-A3). CM SAF Doc. SAF/CM/RMIB/VAL/GAC/TOA, 120 pp., https://www.cmsaf.eu/SharedDocs/Literatur/document/2023/saf_cm_rmib_val_gac_toa_1_1_pdf.html.
- Doelling, D. R., and Coauthors, 2013: Geostationary enhanced temporal interpolation for CERES flux products. *J. Atmos. Oceanic Technol.*, **30**, 1072–1090, <https://doi.org/10.1175/JTECH-D-12-00136.1>.
- Ellingson, R. G., H.-T. Lee, D. Yanuk, and A. Gruber, 1994: Validation of a technique for estimating outgoing longwave radiation from HIRS radiance observations. *J. Atmos. Oceanic Technol.*, **11**, 357–365, [https://doi.org/10.1175/1520-0426\(1994\)011<0357:VOATFE>2.0.CO;2](https://doi.org/10.1175/1520-0426(1994)011<0357:VOATFE>2.0.CO;2).
- Hersbach, H., and Coauthors, 2020: The ERA5 global reanalysis. *Quart. J. Roy. Meteor. Soc.*, **146**, 1999–2049, <https://doi.org/10.1002/qj.3803>.
- Hogan, R. J., and A. Bozzo, 2018: A flexible and efficient radiation scheme for the ECMWF model. *J. Adv. Model. Earth Syst.*, **10**, 1990–2008, <https://doi.org/10.1029/2018MS001364>.
- Johnson, G. C., J. M. Lyman, and N. G. Loeb, 2016: Improving estimates of Earth’s energy imbalance. *Nat. Climate Change*, **6**, 639–640, <https://doi.org/10.1038/nclimate3043>.
- Karlsson, K.-G., and Coauthors, 2013: CLARA-A1: A cloud, albedo, and radiation dataset from 28 yr of global AVHRR data. *Atmos. Chem. Phys.*, **13**, 5351–5367, <https://doi.org/10.5194/acp-13-5351-2013>.
- , and Coauthors, 2017: CLARA-A2: The second edition of the CM SAF cloud and radiation data record from 34 years of global AVHRR data. *Atmos. Chem. Phys.*, **17**, 5809–5828, <https://doi.org/10.5194/acp-17-5809-2017>.
- , and Coauthors, 2023a: CLARA-A3: CM SAF Cloud, Albedo and Surface Radiation dataset from AVHRR data—Edition 3. CM SAF, accessed 1 May 2023, https://doi.org/10.5676/EUM_SAF_CM/CLARA_AVHRR/V003.
- , and Coauthors, 2023b: CLARA-A3: The third edition of the AVHRR-based CM SAF climate data record on clouds, radiation and surface albedo covering the period 1979 to 2023. *Earth Syst. Sci. Data*, **15**, 4901–4926, <https://doi.org/10.5194/essd-15-4901-2023>.
- Knapp, K. R., and Coauthors, 2011: Globally gridded satellite observations for climate studies. *Bull. Amer. Meteor. Soc.*, **92**, 893–907, <https://doi.org/10.1175/2011BAMS3039.1>.
- Kondratovich, V., 2013: GOES Surface and Insolation Products (GSIP), version 3.3. NOAA/NESDIS/STAR System Description Doc. version 1.3., 22 pp.
- Lee, H.-T., A. Gruber, R. G. Ellingson, and I. Laszlo, 2007: Development of the HIRS outgoing longwave radiation climate dataset. *J. Atmos. Oceanic Technol.*, **24**, 2029–2047, <https://doi.org/10.1175/2007JTECHA989.1>.
- , C. J. Schreck, and K. R. Knapp, 2014: Generation of the daily OLR climate data record. 2014 EUMETSAT Meteorological Satellite Conf., Geneva, Switzerland, EUMETSAT.
- Loeb, N. G., B. A. Wielicki, D. R. Doelling, G. L. Smith, D. F. Keyes, S. Kato, N. Manalo-Smith, and T. Wong, 2009: Toward optimal closure of the Earth’s top-of-atmosphere radiation budget. *J. Climate*, **22**, 748–766, <https://doi.org/10.1175/2008JCLI2637.1>.
- , and Coauthors, 2018: Clouds and the Earth’s Radiant Energy System (CERES) Energy Balanced and Filled (EBAF) top-of-atmosphere (TOA) Edition-4.0 data product. *J. Climate*, **31**, 895–918, <https://doi.org/10.1175/JCLI-D-17-0208.1>.
- Schmidt, A., and Coauthors, 2018: Volcanic radiative forcing from 1979 to 2015. *J. Geophys. Res. Atmos.*, **123**, 12 491–12 508, <https://doi.org/10.1029/2018JD028776>.
- Stengel, M., and Coauthors, 2020: Cloud_cci Advanced Very High Resolution Radiometer post meridiem (AVHRR-PM) dataset version 3: 35-year climatology of global cloud and radiation properties. *Earth Syst. Sci. Data*, **12**, 41–60, <https://doi.org/10.5194/essd-12-41-2020>.
- Wielicki, B. A., B. R. Barkstrom, E. F. Harrison, R. B. Lee III, G. L. Smith, and J. E. Cooper, 1996: Clouds and the Earth’s Radiant Energy System (CERES): An Earth observing system experiment. *Bull. Amer. Meteor. Soc.*, **77**, 853–868, [https://doi.org/10.1175/1520-0477\(1996\)077<0853:CATERE>2.0.CO;2](https://doi.org/10.1175/1520-0477(1996)077<0853:CATERE>2.0.CO;2).
- Young, A. H., K. R. Knapp, A. Inamdar, W. Hankins, and W. B. Rossow, 2018: The International Satellite Cloud Climatology Project H-series climate data record product. *Earth Syst. Sci. Data*, **10**, 583–593, <https://doi.org/10.5194/essd-10-583-2018>.
- Zhang, Y., W. B. Rossow, A. A. Lacis, and V. Oinas, 2019: Calculation, evaluation and application of long-term, global radiative flux datasets at ISCCP: Past and present. *Study of Cloud and Water Processes in Weather and Climate through Satellite Observations*, Lectures in Climate Change, Vol. 3, World Scientific, 151–177, https://doi.org/10.1142/9789811256912_0009.